Evidence of intrinsic magnetism in capped ZnO nanoparticles

J. Chaboy,[1,2] R. Boada,[1,2] C. Piquer,[1,2] M. A. Laguna-Marco,[3] M. García-Hernández,[3] N. Carmona,[4] J. Llopis,[4] M. L. Ruíz-González,[5] J. González-Calbet,[5] J. F. Fernández,[6] and M. A. García[6]

[1]*Instituto de Ciencia de Materiales de Aragón, Consejo Superior de Investigaciones Científicas, Universidad de Zaragoza, 50009 Zaragoza, Spain*

[2]*Departamento de Física de la Materia Condensada, Universidad de Zaragoza, 50009 Zaragoza, Spain*

[3]*Instituto de Ciencia de Materiales de Madrid, CSIC, Cantoblanco, 28049 Madrid, Spain*

[4]*Dpto. Física de Materiales, Universidad Complutense de Madrid, 28040 Madrid, Spain*

[5]*Dpto. Química Inorgánica, Universidad Complutense de Madrid, 28040 Madrid, Spain*

[6]*Instituto de Cerámica y Vidrio, Consejo Superior de Investigaciones Científicas, Madrid 28049, Spain*

(Received 23 July 2010; published 11 August 2010)

We present here direct experimental evidence of the magnetic polarization of Zn atoms in ZnO nanoparticles capped with different materials by means of x-ray magnetic circular dichroism (XMCD). Our results demonstrate that the magnetism in this material is intrinsic and relays in the ZnO conduction band. The analysis of both x-ray absorption spectroscopy and XMCD signals points out the formation of a well-defined interface between ZnO and the capping molecule in which the exotic magnetism arises at the hybridized band formed among Zn and the bonding atom of the molecule. The magnetic properties of these systems should critically depend on the details of this interface which may offer a new insight into the different observations for seemingly identical materials.

DOI: 10.1103/PhysRevB.82.064411 PACS number(s): 75.50.Pp, 61.05.cj, 68.47.Gh, 78.70.Dm

I. INTRODUCTION

In the last years, the advances in material science allowed to develop materials with tuned physical properties (mechanical, magnetic, optical, transport, etc.) with great accuracy for specific applications in many fields. Nowadays, the main challenge is probably the development of multifunctional materials combining properties that do not stand together naturally. In this sense, one of the major goals is the coexistence of semiconductor properties and room-temperature ferromagnetism due to the key role of these materials in technological devices. Recently the research on new ferromagnetic semiconductors was focused on the so-called diluted magnetic semiconductors (DMS). However, there is a great controversy around the magnetic properties of DMS at such extent that some authors wonder "if the dilute doping of the oxides with magnetic cations may be something of a smokescreen as far as the magnetism is concerned."[1]

In this situation, nanomaterials can represent an opportunity to develop the desired multifunctional materials exhibiting semiconductor and ferromagnetic properties. The size and surface effects that modify the materials properties at nanoscale, provide a method to tune their physical properties opening the possibility to induce coexistence of properties not achievable at the bulk scale.[2–4] Actually, several recent reports claimed the observation of ferromagnetism in semiconductor and insulating oxide nanostructures without any doping despite the diamagnetic character of the material in bulk.[5–8] Among these, we recently reported the observation of room-temperature ferromagnetism of ZnO nanoparticles (NPs) capped with different molecules.[8] This result was accounted in terms of the modification of the electronic structure induced by the capping molecule: the charge transfer at the bonds created between the NPs surface atoms and the molecules induce a modification of the NP electronic configuration that scaled with the appearance of the magnetic properties of the NPs.

We report here an extensive study of the ZnO NPs capped with different molecules by x-ray absorption spectroscopy (XAS) methods in order to advance in the understanding of this surprising magnetism. Our results confirm that the reported ferromagnetism is intrinsic. Moreover while it is commonly accepted that the ferromagnetism in these oxides arise from the valence band (created from the metallic cations 3*d* orbitals), we demonstrate here that it relays on the conduction band of the semiconductor.

II. EXPERIMENTAL

ZnO NPs were prepared by sol-gel and subsequently capped with three different organic molecules: tryoctylphosphine (TOPO), dodecylamine (AMINE), and dodecanethiol (THIOL), which bond to the particle surface through an O, N, and S atom, respectively. $Zn(Ac)_2$ (5 mmol) was dissolved in dimethyl sulfoxide (DMSO) and the solution was heated and kept at 60 °C under stirring. Then a solution of tetramethylammonium hydroxide pentahydate [TMAH, $N(CH_3)_4OH$, 97%, Sigma-Aldrich], (7.5 mmol) in ethanol was added dropwise. After that, AMINE, THIOL, and TOPO capped nanocrystals were precipitated adding dodecylamine (7.5 mmol), dodecanethiol (7.5 mmol), and TOPO (7.5 mmol) solutions in heated ethanol, respectively, to the precursor solution. The products thus obtained were filtered and washed several times with heated ethanol. The recovered powders were allowed to dry at room temperature.

The materials used for the synthesis were: Zinc acetate dihydrate [$Zn(Ac)_2$, $Zn(CH_3CO_2)_2 \cdot 2H_2O$, 98%, Sigma-Aldrich, ≤ 5 ppm of Fe impurities], tetramethylammonium hydroxide pentahydrate [TMAH, $N(CH_3)_4OH$, 97%, Sigma-

Aldrich), (DMSO, $(CH_3)_2SO$, Sigma-Aldrich], dodecylamine ($C_{12}H_{25}NH_2$, ≥98%, Merck), dodecanethiol ($C_{12}H_{25}SH$, 98%, Sigma-Aldrich), tetraoctylphospine oxide [TOPO, $(C_8H_{17})_3PO$, 90% technical grade, Sigma-Aldrich] and absolute ethanol (CH_3CH_2OH, Panreac) were used as received.

Photoluminescence (PL) excitation and emission spectra were recorded with a Perkin-Elmer LS-5 spectrofluorometer performing the appropriate correction for the lamp intensity and photomultiplier spectral response. Powder samples were placed in a circular sampleholder and covered with a quartz window. No significant contribution from the sampleholder or from the quartz window to the emission or excitation bands in the spectral region of interest was found. Reflectance was measured with a Shimadzu 3100 monochromator with an integrating sphere attached to collect both specular and diffuse reflectance using the same sampleholder than for the PL measurements. No significant contribution of the sample holder nor from the window was found.

Magnetic measurements were performed on dried nanocrystal powder samples using a Quantum Design superconducting quantum interference device (SQUID) magnetometer. All possible sources of experimental errors described in Ref. 9 were considered and avoided. Samples (always handled with nonmetallic tools) were placed into a gelatin capsule and mounted on straws. A gelatin capsule without any powder was also mounted on a straw and measured for control. Zn precursor (Zinc acetate dihydrate) was measured to detect contamination in starting powder. For selected samples, several masses were measured in order to determine whether the magnetic signal scales with the mass.

Zn $L_{2,3}$-edges x-ray magnetic circular dichroism (XMCD) signals were recorded at the intermediate x-ray branch of the 4-ID beamline of the APS Facility.[10] Measurements were made in both fluorescence and total electron yield. No XMCD signal was observed independently of the detection mode. Zn *K*-edge XAS and XMCD experiments were performed at the beamline BL39XU of the SPring8 Facility.[11] XMCD spectra were recorded in the transmission mode by using the helicity-modulation technique. The sample is magnetized by an external magnetic field applied in the direction of the incident beam and the helicity is changed from positive to negative each energy point. For sake of accuracy the direction of the applied magnetic field is reversed and XMCD is recorded again by switching the helicity. The subtraction of the XMCD spectra recorded for both field orientations cancels, if present, any spurious signal. The absorption spectra were analyzed according to standard procedures: the origin of the energy scale, E_0, was chosen at the inflection point of the absorption edge and the spectra were normalized to the averaged absorption coefficient at high energy.

The computation of the Zn *K*-edge XANES spectra was carried out using the multiple-scattering code CONTINUUM.[12] A complete discussion of the procedure can be found elsewhere.[13,14] The computations have been initially performed for bulk ZnO. We have built up a cluster (177 atoms) containing the scattering contributions from all the atoms within a coordination sphere of 8 Å around the absorbing Zn. The potential for the cluster was approximated by a set of spherically averaged muffin-tin potentials built by following the standard Mattheis' prescription. The muffin-tin radii were determined following the Norman's criterion and by using a 1% overlapping factor. The calculated theoretical spectra have been further convoluted with a Lorentzian shape function ($\Gamma = 1.5$ eV) to account for the core-hole lifetime[15] and the experimental resolution. It was found during the calculations the real Dirac-Hara exchange and correlation potential leads to the best agreement both in energy and intensity, between the experimental and theoretical XANES spectra.

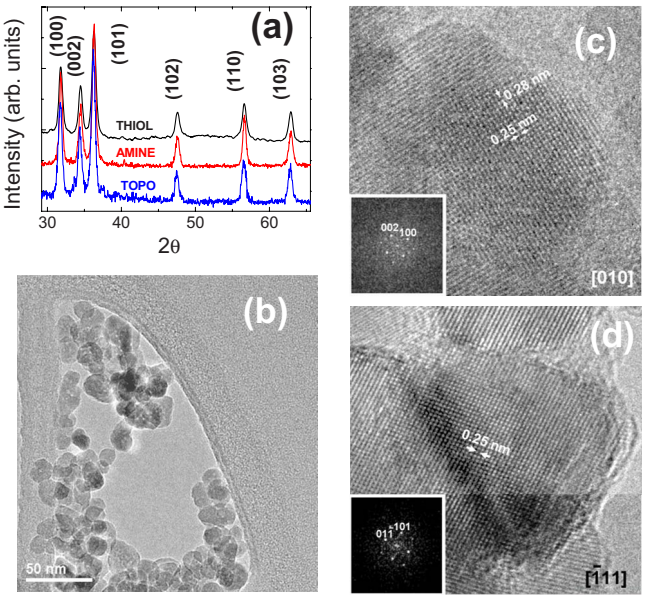

FIG. 1. (Color online) (a) X-Ray diffraction patterns of the AMINE, THIOL, and TOPO samples; The maxima (labeled) in the pattern are indexed on the basis of a ZnO wurtzite-type unit cell. The particle size calculated from the peaks in the figure using the Debye-Scherrer formula resulted 20.8 ± 2.5 nm, 19.5 ± 1.5 nm, and 19.06 ± 2.6 nm for the THIOL, AMINE, and TOPO, respectively. (b) Low magnification image of the TOPO sample evidencing an average size around 20 nm. [(c) and (d)] HREM images and corresponding FT (inset) are in agreement to the wurzite lattice.

III. RESULTS AND DISCUSSION

A. Characterization of the samples

We have performed a detailed characterization of the samples by using different characterization techniques.

1. X-ray diffraction (XRD) and HR-transmission electron microscopy (TEM) characterization

Structural characterization was performed by means of XRD and TEM (see Fig. 1). For the three cases, the formation of hexagonal ZnO nanoparticles with average size around 20–30 nm is evidenced. Energy dispersive spectroscopy analysis agrees with the presence of ZnO and it excludes the presence of magnetic impurities within the sensitivity (0.01) of this technique. This is also confirmed by the PL spectra.

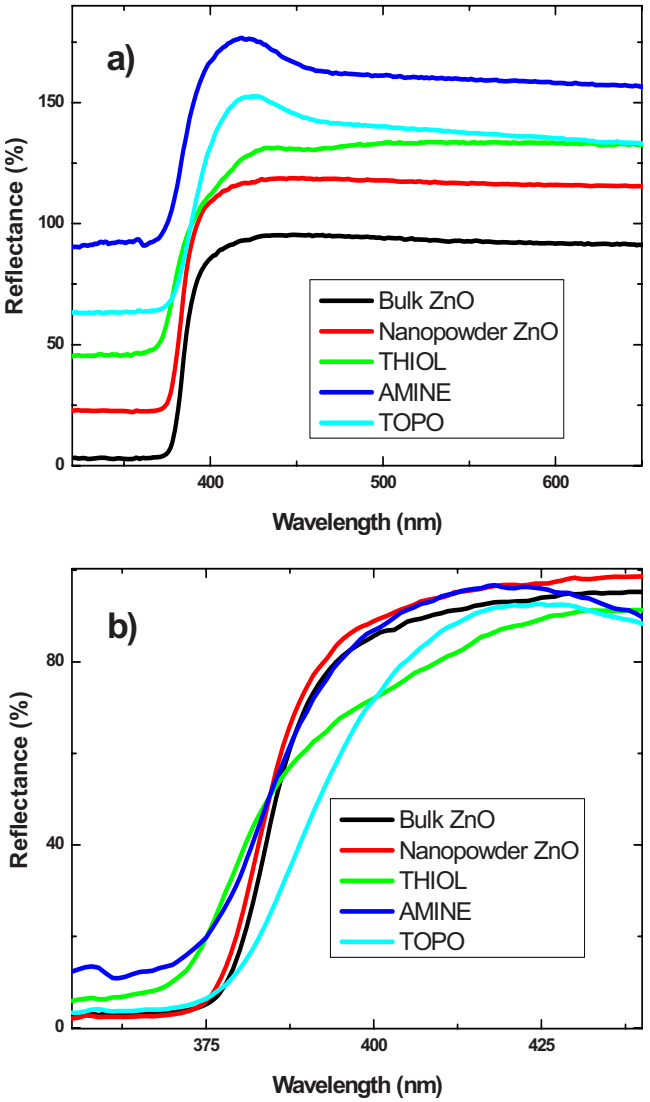

FIG. 2. (Color online) (a) Diffuse reflectance spectra for the ZnO nanoparticles capped with different molecules. Bulk ZnO and nanopowders are also shown for comparison purposes. Curves are vertically displaced for clarity. (b) Detail of the band-gap profile.

2. Optical absorption and photoluminescence

As ZnO is a degenerated semiconductor with an energy gap (3.35 eV) in the UV-Vis part of the spectrum, optical spectroscopy probing transitions between valence and conduction band provides useful information about its electronic structure. Figure 2 shows the integrated reflectance of the samples in the 350–650 nm range. Bulk ZnO exhibits a typical plain profile at the visible part of the spectrum with a sharp decay at about 400 nm reflecting the ZnO bandgap. A reference sample of ZnO nanopowder (particle size $<$50 nm) presented a very similar spectrum with slight modifications at the gap energy. ZnO nanoparticles exhibit also the reflectance decay at the bandgap, confirming they retain the semiconductor character of ZnO. However, clear differences at the edge region are found with respect to the bulk and nanopowder ZnO. The nanoparticles shows an increase in reflectance close to the edge (around 420 nm) indicative of a different electronic structure at the bottom of the conduction band. In addition, the bandgap decay results sharper for the bulk and nanopowder while the nanoparticles exhibit a wider profile indicative of a more heterogeneous material and also a different density of available states. As it will be discussed later on in the text, the heterogeneity detected for the nanoparticles is in agreement with the formation of a layer at the particle surface. The dependence of the bandgap profile with the molecule in addition to the fact that this feature is absent in the ZnO uncapped nanopowder indicates that it is related to the formation of the bonds at the particle surface.

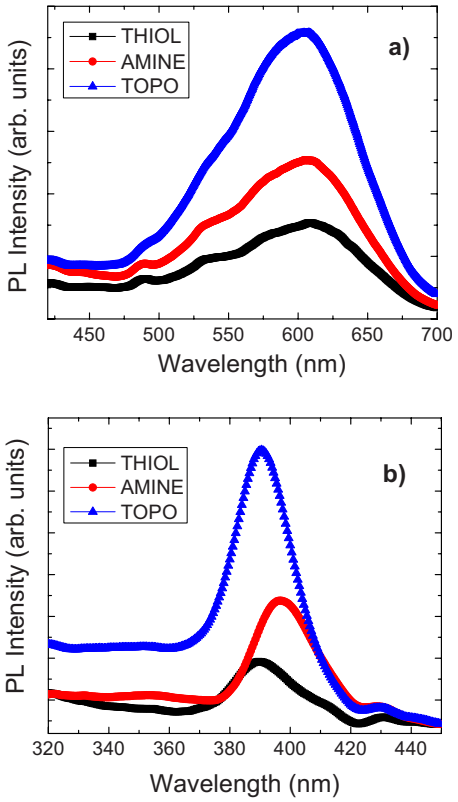

FIG. 3. (Color online) (a) Emission spectra upon excitation with 320 nm light. (b) Excitation spectra for the 570 nm emission.

The photoluminescence spectra of the ZnO NPs are reported in Fig. 3. The emission spectra upon excitation with 320 nm light shows a broad band centered at about 600 nm for the three samples. This emission is shifted with respect to the typical emission of bulk ZnO (centered at 550 nm) and its intensity depends on the capping molecule. This emission band is ascribed to an energy level induce by the presence of defects in ZnO. Although the particular defect responsible for the emission is still under discussion, it is commonly accepted that oxygen vacancies are involved.[16] The excitation spectra for the 570 nm emission exhibit a narrow peak at about 390 nm which correspond to the ZnO bandgap (see Fig. 2). The spectra shows variations in intensity and a slight shifts depending on the capping molecule, peaking at 389 nm for THIOL, 397 nm for AMINE, and 390 for TOPO. The changes in the photoluminescence features are indicative of differences in the electronic configuration of the particle depending on the capping molecule. In particular, surface states

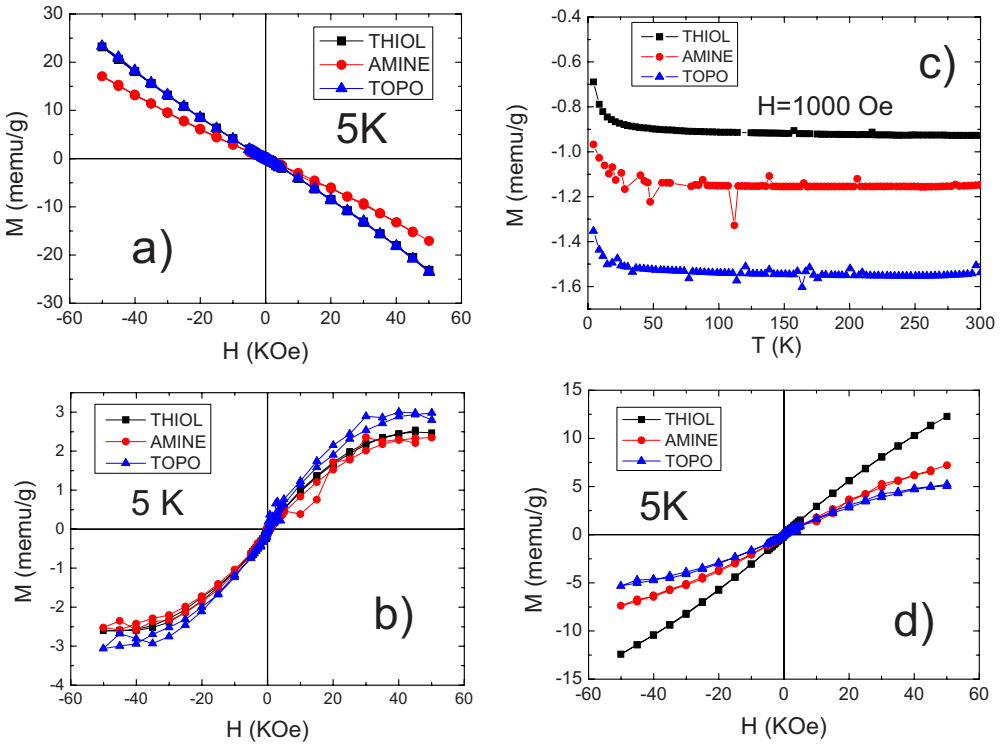

FIG. 4. (Color online) (a) Magnetization curves of the ZnO nanoparticles capped with different molecules. (b) Curves after subtracting a linear background. (c) Thermal dependence of the magnetization under an applied field of 1000 Oe. (d) Magnetization curves showing the paramagnetic and ferromagnetic components (subtracting the diamagnetism).

are known to provide an alternative decay path for excited electrons; thus the changes in the PL intensity are associated with the presence and concentration of these surface states that will be determined by the bonds established between the ZnO particle and the capping molecule.

3. Magnetic characterization

Figure 4 summarizes the results of the SQUID measurements. Samples exhibit an overall diamagnetic behavior at 5 K [Fig. 4(a)]. However, the thermal dependence of the magnetization [Fig. 4(b)] points out the existence of a paramagnetic signal following Curie-Weiss law. The diamagnetic and paramagnetic susceptibility at 5 K can be determined separately assuming that this later is negligible at 300 K (as the M vs T curve is flat at this temperature) and the diamagnetic contribution is thermally independent. Subtracting a linear background, it is observed the existence of an additional nonsaturated and ferromagneticlike contribution that is presented in Fig. 4(c). By "ferromagneticlike" behavior we mean that the magnetization curves of these samples show most of the typical features of ferromagnetic materials (remanence, coercivity, saturation) but not the presence of exchange interaction responsible of the magnetic order that is hard to understand in these materials. This ferromagneticlike contribution shows hysteresis, remanence, and coercivity ($H_C \sim 200$ Oe) which remain almost identical at high temperature. The value of the saturation magnetization, ~ 2 memu/g, is in agreement with the values previously reported although the dependence with the capping molecule is fairly different.[8] From Fig. 4(d), where the magnetization curves at 5 K after subtracting the diamagnetic component are shown, it is observed that the paramagnetic contribution is fairly larger than the ferromagnetic one.

The magnetization curves of the sample holder used for the measurements (gelatin capsule plus plastic straw) are shown in Fig. 5. It exhibits a diamagnetic behavior at both 5 and 300 K. Moreover, the Curie-Weiss decay observed for the sample holder is 50 times smaller than for the THIOL sample. After subtracting a linear background the magnetization curves shows also ferromagneticlike component but it is at least five times smaller than that of any of the samples at $T=5$ K. Moreover, differently to the samples (see Fig. 6) it strongly decays at high temperature being more than 20 times smaller at 300 K while the observed decrease in the samples is significantly smaller. Finally, it should be noted that, as shown in Fig. 5, when normalized to the mass the ferromagnetic component of the samples overlap indicating this signal is not a background but really arises from the sample. SQUID measurements on the precursor found no magnetic signal up to a resolution of 5×10^{-5} emu/g that is two orders of magnitude smaller than the ferromagneticlike signal reported here. The thermal dependence of the magnetization resulted different for each capping molecule highlighting the influence of the surface bonds in this magnetism. In agreement with the reflectance measurements these results suggest a correlation between the nature of the bonds formed at the particle surface and the appearance of magnetism.

B. XMCD and XAS results

In order to investigate the origin of the ferromagnetic signals measured with the SQUID, we have performed a com-

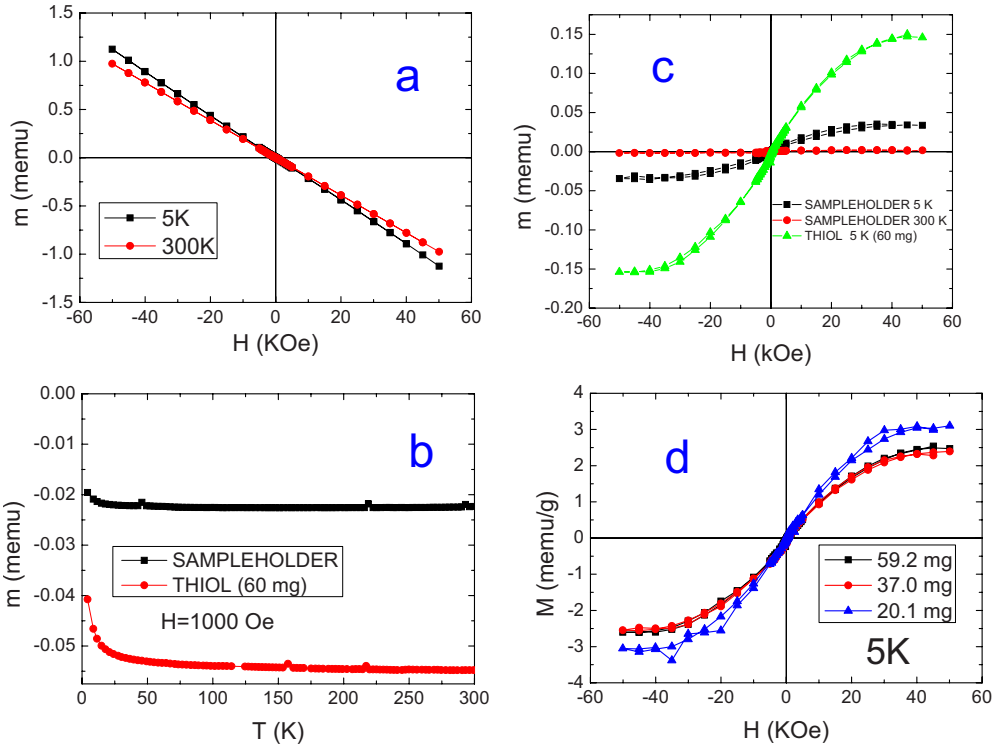

FIG. 5. (Color online) (a) Magnetization curves of the sample holder used for the measurements. (b) Thermal dependence of the magnetization (curve for THIOL sample is also presented for comparison purposes). (c) Magnetization curves after subtracting a linear background. Curve for THIOL at 5 K is also presented for comparison purposes. (d) Ferromagnetic component for the THIOL sample at 5 K measured on three different specimen of 20 mg, 40 mg, and 60 mg.

bined XAS and XMCD study a the Zn *K* edge in the same samples. It should be noted that the element specificity of XMCD guaranties the absence of extrinsic contributions to the measured magnetic signals.

Figure 7(a) reports the XAS and XMCD spectra recorded at the Zn $L_{2,3}$ edges of the AMINE sample. No XMCD signal could be observed in the measured energy region, down to the noise level, in agreement with previous works.[17–19] By contrast to the $L_{2,3}$ case, a clear XMCD signal is found at the Zn *K* edge [Fig. 7(b)]. These results unambiguously prove that the 3*d* electronic shells of Zn do not carry any measurable ferromagnetic moment and that the presence of defects and vacancies do not yield a partially unfilled magnetically polarized 3*d* shell. It should be noted that if the polarization of the Zn *p* states is due to the existence of a 3*d* Zn magnetic moment the XMCD effect at the Zn $L_{2,3}$ edges would be well above the detection limit.[20] The intensity of the XMCD at the *K* edge of transition metals is typically more than two orders of magnitude smaller than at the $L_{2,3}$ edges.[21,22] Taking into account that the magnitude of the Zn *K*-edge XMCD is $\sim 2.5 \times 10^{-4}$ the expected XMCD at the Zn $L_{2,3}$ edges should be greater than 10^{-2}, i.e., within the present sensitivity limit at third generation sources.

This result evidences, on the one hand, the intrinsic nature of the magnetism of Zn atoms in these capped ZnO NPs. Moreover, as the x-ray absorption at the Zn *K*-edge probes the empty *p* states of Zn (actually 4*sp* due to hybridization) this result also indicates that the magnetic polarization of the Zn atoms takes place at the *sp* conduction band, i.e., it is *p* magnetism. Therefore, the absence of XMCD signal at the Zn $L_{2,3}$ edges cannot be identified with the absence of Zn magnetization but only of 3*d* Zn magnetic moments. Indeed, if the observed magnetism is associated with the creation of oxygen 2*p* holes, the *sp* band of Zn should be also concerned due to the hybridization of both orbitals in ZnO. Hence, the Zn *K*-edge XMCD should directly reflect, in agreement with our findings, the magnetic polarization of these electronic states.[23]

The dependence of the XMCD signal at 10 T with the capping molecule is also in agreement with the value of the ferromagnetic component measured with the SQUID. The largest magnetization is found now for the TOPO sample while THIOL one exhibit the smallest magnetic signal. Moreover, as shown in Fig. 7(c), the XMCD signal for the THIOL sample increases with the applied magnetic field confirming the existence of a paramagnetic signal; on the contrary the experimental resolution does not allow to confirm the existence a of ferromagnetic signal nor the presence of hysteresis or coercivity. Anyway, the field dependence is an agreement with the SQUID data presented in Fig. 4(d). As XMCD probes only magnetic polarization in the Zn 4*sp* orbital, the diamagnetism coming from Zn filled orbital and other atoms in the sample will not contribute and therefore a mixture of paramagnetism and ferromagnetism could be expected.

While the intensity of the Zn *K*-edge XMCD signals in the AMINE, TOPO, and THIOL samples is similar, the shape of the spectra shows interesting differences that mimics the XAS behavior. A more detailed analysis of the XAS spectra shows for all the samples a prominent peak (B) centered at

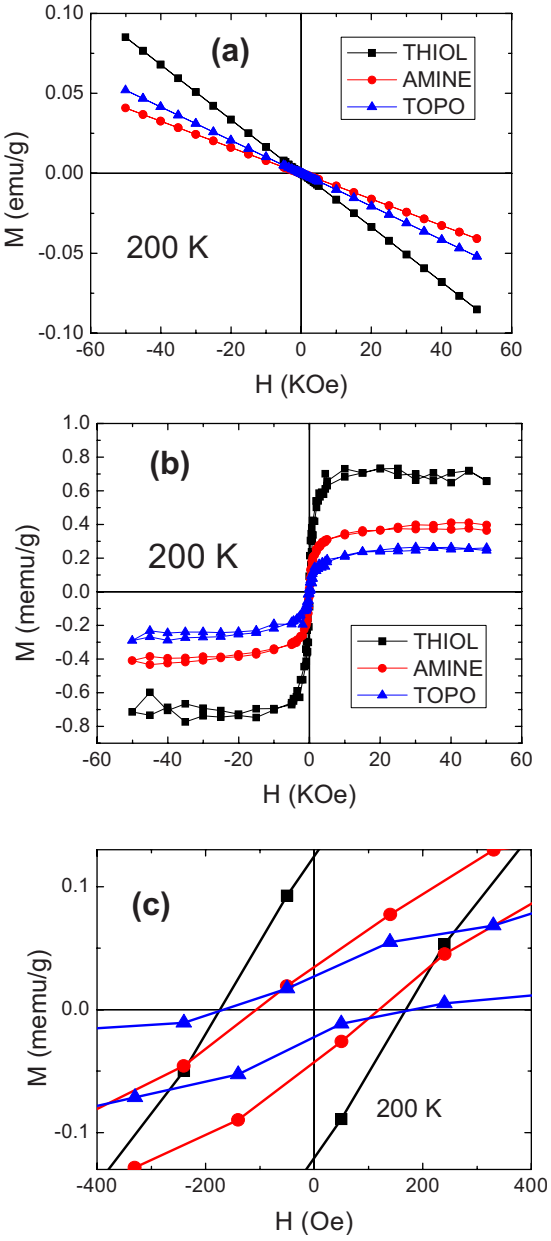

FIG. 6. (Color online) (a) Magnetization curves measured at 200 K. (b) Curves after subtracting a linear background showing the presence of a ferromagneticlike component. The value of this FM-like component is typically 3–4 times smaller than that measured at 5 K. (c) Detail of the low-field region demonstrating the existence of remanence and hysteresis with coercive field on the order of 100 Oe.

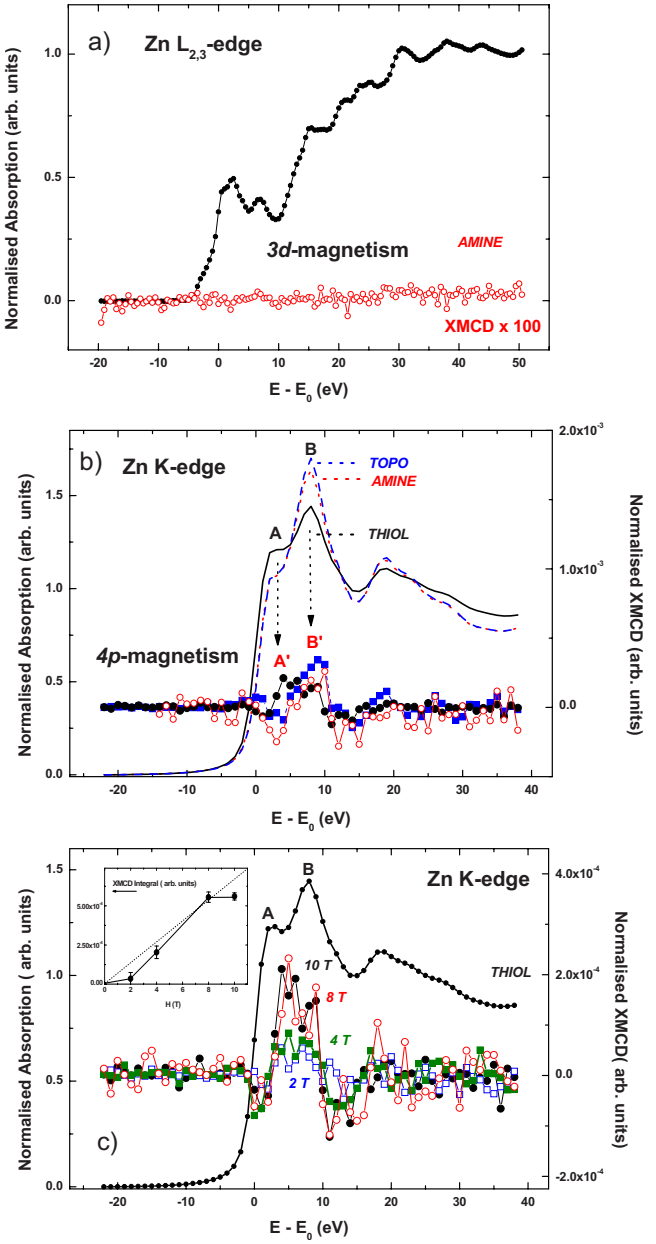

FIG. 7. (Color online) (a) XAS (black) and XMCD (red) Zn $L_{2,3}$-edges spectra for ZnO nanoparticles capped with AMINE recorded at $T=10$ K and with an applied magnetic field of 5 T. (b) Zn K-edge XAS (lines) ad XMCD spectra (symbols) recorded at $T=4.2$ K and $H=10$ T in the case of ZnO NPs capped with AMINE (red, dots), TOPO (blue, dashes), and THIOL (black, solid line). (c) Comparison of the normalized Zn K-edge XMCD spectra recorded as function of the applied magnetic field at $T=4.2$ K in the case of ZnO NPs capped with thiol: 2 T (blue, □), 4 T (green, ■), 8 T (red, ○), and 10 T (●). The dependence of the integrated XMCD signals on the applied magnetic field is shown in the inset.

~8 eV above the absorption edge and shoulderlike feature (A) in the lower energy side [Fig. 7(b)]. At the same energies, XMCD spectra show peaks A′ and B′. TOPO and AMINE display nearly identical XAS and XMCD spectra being slightly different to those of THIOL. In this case the peak A intensity enhances while that of peak B is significantly reduced. Similarly, the XMCD of THIOL shows a reduction in peak B′ and peak A′ becomes positive, resembling the enhancement of the peak A intensity in the XAS spectra. The modification of the XAS profile is often accounted for in terms of changes in the electronic structure.[24]

However, the modification of both the spectral shape and the intensity of the main absorption features cannot be ascribed only to electronic effects since the latter are intimately linked to the local structure.[13] The magnitude of the observed differences between the Zn K-edge XAS spectra of THIOL and those of AMINE and TOPO suggests that structural effects have to be taken into account to understand the XAS behav-

ior. Indeed, the observed variation in the XANES, magnetization and photoluminescence spectra through the TOPO-AMINE-THIOL is just the opposite to that previously reported on similar samples.[8] This result points out that the magnetic behavior is not associated with the electronegativity of the surrounding atoms, as previously proposed,[8] but to the particular structural arrangement of these bonds at the surface of the NPs.

The bond of the surfactant molecule to the ZnO particle takes place at the surface. Therefore, two different Zn atoms contribute to the *K*-edge absorption, i.e., those at the core of the particle and those at the surface in which new Zn-N and Zn-S bonds and Zn-O ones with a modified interatomic distance respect to bulk ZnO can exist depending of the capping. The x-ray absorption in the hard energy region probes both classes of Zn atoms in the NPs and not only those close to the surface. Consequently, the measured Zn *K*-edge spectra would correspond to the addition, with the proper weighting, of the absorption spectra of both Zn species showing different local structure. We have performed a detailed *ab initio* calculation of the Zn *K*-edge XAS aimed to determine the influence of the different coordination induced by the capping. This computational scheme has been applied on a ZnO cluster, including coordination shells within the first 8 Å around Zn (177 atoms) and for a second one (ZnO-S) in which the O atoms of the first coordination shell are substituted by S ones being the Zn-S interatomic distance that of ZnS (wurzite). As shown in Fig. 8, despite only these four atoms have been changed in the cluster the intensity ratio of peaks A and B is inverted in both ZnO and ZnO-S calculations, which mimics the experimental differences of the Zn *K*-edge XAS of both bulk ZnO and THIOL samples. In order to verify that in the latter case both ZnO and ZnS coordination schemes coexist we have constructed a spectrum by adding both ZnO and ZnO-S calculated spectra with a 50% weighting factor. As shown in Fig. 3 the theoretical spectrum reproduces the experimental spectra of both ZnO and THIOL sample, especially regarding the A/B intensity ratio. These results suggest that the observed differences of the XAS spectra are due to the formation of an interface in which the Zn atoms bond to the S atoms of the capping molecule. In principle, it should be expected that the molecules bond to the ZnO surface through single bonds in which one S atom from the molecule substitutes one O of the ZnO particle. However, the *ab initio* XAS computations performed by substituting progressively the four next neighbors oxygen atoms by S ones, see Fig. 8(b), suggest that some Zn atoms could be bonded to more than a single S atom. Our results render a picture in which an interface of Zn atoms bonded to S atoms of the capping molecule consolidates at the surface of the ZnO nanoparticles.

Therefore, the modification of the XAS profile observed in the capped NPs can be explained as due to the surface layer created at the interface between the NPs and the molecules. As the main changes in the XAS profile [peaks A and B in Fig. 7(b)] matches the observed peaks in XMCD spectra and they scale with the magnetic signal measured both by SQUID and XMCD, we conclude that the formation of this surface layer is in the origin of the observed magnetism. Moreover, the formation of this layer will involve mainly

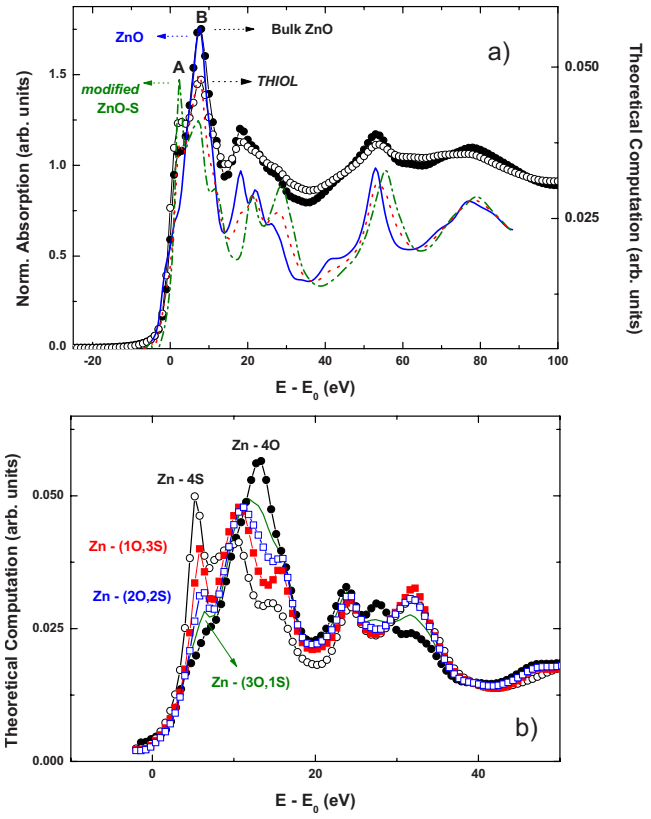

FIG. 8. (Color online) (a) Comparison of the experimental Zn *K*-edge XANES spectra of bulk ZnO (●) and thiol-capped sample (○) and the theoretical spectra calculated on a ZnO cluster (blue, solid line) and the same ZnO cluster in which the O neighbors have been substituted by S at greater distance (green, dotted-dashed) The red dotted line corresponds to the addition of both spectra with a relative weight of 50%. (b) Comparison of the theoretical Zn *K*-edge XANES spectra of the ZnO cluster (●) and the same cluster in which the four next neighbors oxygen atoms have been progressively substituted by S: Zn-(3O,1S) (green, solid line), Zn-(2O,2S) (blue, □), Zn-(1O,3S) (red, ■), and Zn-4S (○).

bonds through Zn 4*sp* orbital, and therefore, the magnetic polarization should relay on this orbital as it is found in the XMCD study. Photoluminescence and optical absorption spectra, both probing transitions involving ZnO conduction band, confirmed the relationship between the modification of ZnO band structure and the appearance of magnetism in the NPs.

To some extent these findings answer the question posed by Keavney and co-workers in their study of Cu-doped ZnO: *Where does the spin reside in ferromagnetic Cu-doped ZnO*?[17] These authors performed an accurate study of the XMCD at Cu 3*d*, O 2*p*, and Zn 3*d* states individually. They find a paramagnetic component originating from the Cu 3*d*, and no magnetic signal in the O or Zn. The only states not probed in this experiment were the Zn 4*p* because it did seem unlikely that all the spin could reside there. The fact that we found a clear XMCD signal at the Zn *K*-edge (probing 4*sp* orbital) while no signal is detected at $L_{2,3}$ edges indicates that the magnetic polarization relays on the ZnO conduction band. This finding represents a breakthrough with the commonly accepted view of magnetism in 3*d* semicon-

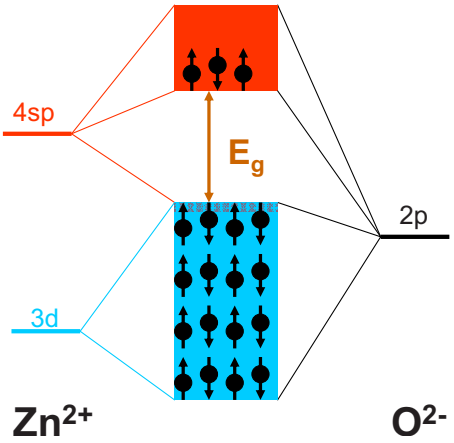

FIG. 9. (Color online) Scheme of the ZnO band structure.

ductor oxides. In the well-known magnetic transition metals as Fe, Co, and Ni and their oxides, the magnetism relays on the cation 3*d* band. Therefore, the appearance unexpected magnetism in transition metal oxides as TiO_2, HfO, or ZnO has been commonly accounted assuming that the magnetic interaction arise from the cation 3*d* orbital and therefore on the valence band of the oxide and mediated by holes. However, our findings demonstrate that the magnetic moment relays on the 4*sp* orbital of the Zn and consequently the magnetism is due to the conduction band.

According to Refs. 25 and 26 the valence band of ZnO is mainly formed by hybridization of Zn 3*d* orbital with O 2*p* ones and there is also a small contribution of ZnO 4*sp* orbital. Therefore, conduction band arise from hybridization of 4*sp* states of Zn ions with a small contribution O 2*p* orbitals (see Fig. 9 for a scheme of the band structure in ZnO). This band can be modified by surface bonds providing a way to tune the magnetic properties of nanoparticles. Therefore, the appearance of magnetism in DMS can be related to the modifications induced in the conduction band by the presence of the doping cations and not due to their magnetic character.[27,28]

IV. SUMMARY AND CONCLUSIONS

We have presented here an extensive study of the ZnO NPs capped with different molecules by using different experimental techniques. X-ray magnetic circular dichroism results demonstrate that the magnetism in these materials is intrinsic and relays in the ZnO conduction band. Moreover, both XAS and XMCD signals point out the formation of a well-defined interface between ZnO and the capping molecule in which the exotic magnetism arises at the hybridized band formed among Zn and the bonding atom of the molecule. Accordingly, the occurrence of magnetism should be related to the structural modification at the interface between the NPs and the molecules rather to the specific electronegativity of the atoms involved in the bonds at this interface.

Contrary to the commonly accepted view, the magnetism arise at the oxide conduction band, opening a via to explain the surprising results find in this field, sometimes seemingly irreconcilable. However, the origin of exchange interactions and/or anisotropy leading to the ferromagneticlike behavior in these nanostructures remains unknown and represents a key challenge in the search for magnetic semiconductors.

ACKNOWLEDGMENTS

This work was partially supported by Spanish CICYT under Grants No. MAT2008-06542-C04-01, No. MAT2008-06517-C02-01, No. CSD2009-00013, and No. FIS-2008-06249, and by the EU project "BONSAI" (Grant No. LSHB-CT-2006-037639). The synchrotron radiation experiments were performed at SPring-8 (Proposals No. 2008B1773 and No. 2009B0024) and APS (Proposal No. GUP-10283). We acknowledge to N. Kawamura, M. Suzuki, and M. Mizumaki, and to J. Freeland for their assistance during the SR experiments at SPring-8 and APS, respectively. R.B. acknowledges the Ministerio de Eduación y Ciencia of Spain for a PhD. Grant. M.A.L. acknowledges the Ministerio de Ciencia e Innovación of Spain for a Juan de la Cierva grant.

[1] J. M. D. Coey, Curr. Opin. Solid State Mater. Sci. **10**, 83 (2006).
[2] Y. Yamamoto, T. Miura, M. Suzuki, N. Kawamura, H. Miyagawa, T. Nakamura, K. Kobayashi, T. Teranishi, and H. Hori, Phys. Rev. Lett. **93**, 116801 (2004).
[3] T. Shinohara, T. Sato, and T. Taniyama, Phys. Rev. Lett. **91**, 197201 (2003).
[4] P. Esquinazi, D. Spemann, R. Höhne, A. Setzer, K. H. Han, and T. Butz, Phys. Rev. Lett. **91**, 227201 (2003).
[5] I. Carmeli, G. Leitus, R. Naaman, S. Reich, and Z. Vager, J. Chem. Phys. **118**, 10372 (2003).
[6] J. M. D. Coey, M. Venkatesan, and C. B. Fitzgerald, Nature Mater. **4**, 173 (2005).
[7] K. R. Kittilstved, W. K. Liu, and D. R. Gamelin, Nature Mater. **5**, 291 (2006).
[8] M. A. García *et al.*, Nano Lett. **7**, 1489 (2007).
[9] M. A. García, E. F. Pinel, J. de la Venta, A. Quesada, V. Bouzas, J. L. Fernández, J. L. Romero, M. S. Martín-González, and J. L. Costa-Krämer, J. Appl. Phys. **105**, 013925 (2009).
[10] J. W. Freeland, J. C. Lang, G. Srajer, R. Winarski, D. Shu, and D. M. Mills, Rev. Sci. Instrum. **73**, 1408 (2002).
[11] H. Maruyama, J. Synchrotron Radiat. **8**, 125 (2001).
[12] C. R. Natoli and M. Benfatto (unpublished).
[13] J. Chaboy, J. Synchrotron Radiat. **16**, 533 (2009).
[14] J. Chaboy and S. Quartieri, Phys. Rev. B **52**, 6349 (1995).
[15] M. O. Krause and J. H. Oliver, J. Phys. Chem. Ref. Data **8**, 329 (1979).
[16] A. van Dijken, E. A. Meulemkamp, D. Vanmaekelbergh, and A. Meijerink, J. Phys. Chem. B **104**, 1715 (2000).
[17] D. J. Keavney, D. B. Buchholz, Q. Ma, and R. P. H. Chang, Appl. Phys. Lett. **91**, 012501 (2007).
[18] A. Barla *et al.*, Phys. Rev. B **76**, 125201 (2007).
[19] M. Gacic, G. Jakob, C. Herbort, H. Adrian, T. Tietze, S. Bruck,

and E. Goering, Phys. Rev. B **75**, 205206 (2007).
[20] J. Chakhalian *et al.*, Nat. Phys. **2**, 244 (2006).
[21] J. Chaboy, L. M. García, F. Bartolomé, A. Marcelli, G. Cibin, H. Maruyama, S. Pizzini, A. Rogalev, J. B. Goedkoop, and J. Goulon, Phys. Rev. B **57**, 8424 (1998).
[22] L. M. García, J. Chaboy, F. Bartolomé, and J. B. Goedkoop, Phys. Rev. Lett. **85**, 429 (2000).
[23] J. Chaboy, H. Maruyama, L. M. García, J. Bartolomé, K. Kobayashi, N. Kawamura, A. Marcelli, and L. Bozukov, Phys. Rev. B **54**, R15637 (1996).
[24] P. Crespo, R. Litrán, T. C. Rojas, M. Multigner, J. M. de la Fuente, J. C. Sánchez-López, M. A. García, A. Hernando, S. Penadés, and A. Fernández, Phys. Rev. Lett. **93**, 087204 (2004).
[25] K. Matsunaga, F. Oba, I. Tanaka, and H. Adachi, J. Electroceram. **4**, 69 (1999).
[26] A. B. Anderson and A. Nichols, J. Am. Chem. Soc. **108**, 1385 (1986).
[27] N. Sanchez, S. Gallego, and M. C. Muñoz, Phys. Rev. Lett. **101**, 067206 (2008).
[28] S. Gallego, J. I. Beltrán, J. Cerdá, and M. C. Muñoz, J. Phys.: Condens. Matter **17**, L451 (2005).